Construction and Building Materials

Cementation anisotropy associated with microbially induced calcium-carbonate precipitation and its treatment effect on granular soils

--Manuscript Draft--

Manuscript Number:	CONBUILDMAT-D-23-02883
Article Type:	Research Paper
Keywords:	Granular soils; Microbially induced calcium-carbonate precipitation; Cementation anisotropy; Treatment effect
Corresponding Author:	Bo Zhou Wuhan, CHINA
First Author:	Xing Zhang
Order of Authors:	Xing Zhang
	Bo Zhou
	Lingyun You
	Ziyang Wu
	Huabin Wang
Abstract:	Microbially induced calcium-carbonate precipitation (MICP) can help cement sand particles together and has emerged as a promising alternative to traditional ground-improvement treatments for granular soils. Owing to precipitation and absorption in different directions, MICP leads to anisotropic cementation. This study was aimed at examining the mechanism of cementation anisotropy and its treatment effect on two commonly used granular soils in geotechnical engineering: quartz sand and calcareous sand. A novel MICP technique was used to prepare bio-cemented sand specimens with different anisotropic patterns of cementation. Microscopic detection techniques were applied to examine the microstructure of the produced MICP cementation. The cementation in the vertical and horizontal directions was different, owing to gravity. The granular surface properties affected the content, morphology, and cement force of the bio-cements produced by MICP treatment. The results of unconfined compression strength experiments confirmed the occurrence of cementation anisotropy and its substantial effects on the stiffness, strength, and fracture patterns of MICP-treated quartz sand and calcareous sand. These findings can help to clarify the formation mechanism of bio-cements and promote the optimised application of MICP for the treatment of granular soils.
Suggested Reviewers:	Chaosheng Tang, PhD Professor, Nanjing University tangchaosheng@nju.edu.cn
	Yang Xiao, PhD Professor, Chongqing Medical University hhuxyanson@163.com
	Aboelkasim Diab, PhD Associate Professor, Aswan University adiab@aswu.edu.eg
	MOHD ROSLI MOHD HASAN, PhD Associate Professor, Universiti Sains Malaysia cerosli@usm.my
	Huailei Cheng, PhD The Hong Kong Polytechnic University huai-lei.cheng@polyu.edu.hk

School of Civil and Hydraulic Engineering
Huazhong University of Science and Technology
Wuhan, China

20 March 2023

Dear Editor,

I am pleased to submit a manuscript entitled 'Cementation anisotropy associated with microbially induced calcium-carbonate precipitation and its treatment effect on granular soils' by Xing Zhang, Bo Zhou, Lingyun You, Ziyang Wu, Huabin Wang. We would like the paper to be reviewed as an article for possible publication in *Construction and Building Materials*. It is an original paper which has neither been previously published nor simultaneously been submitted to anywhere else, in English or in any other language.

This research presents a detailed study on the mechanism of cementation anisotropy and its (Microbially induced calcium-carbonate precipitation) MICP treatment effect on quartz sand and calcareous sand. A novel MICP method was proposed. The findings and results are sure to be of interest to researchers studying on the MICP and micromechanics of granular soils.

Correspondence regarding this paper should be directed to:
Dr. Bo Zhou
School of Civil and Hydraulic Engineering
Huazhong University of Science and Technology
Please e-mail at zhoubohust@hust.edu.cn

Thank you very much for your attention and we look forward to hearing from you.

Yours sincerely and best wishes,

Bo Zhou

Cementation anisotropy associated with microbially induced calcium-carbonate precipitation and its treatment effect on granular soils

Xing Zhang[12], Bo Zhou[1*], Lingyun You[1], Ziyang Wu[1], Huabin Wang[1]

[1]School of Civil and Hydraulic Engineering,
Huazhong University of Science and Technology,
Wuhan, China

[2] School of Computer Science and Engineering,
Nanyang Technological University,
Singapore

*Corresponding author:
Dr Bo Zhou, zhoubohust@hust.edu.cn

Highlights

1. A novel MICP treatment for specimens with cementation anisotropy
2. Insight into MICP-produced anisotropic cementation induced by gravity and surface absorption
3. Comparison of distinct MICP treatment mechanisms between quartz sand and calcareous sand
4. Significant effect of cementation anisotropy on mechanical properties of bio-cemented sands

Abstract

Microbially induced calcium-carbonate precipitation (MICP) can help cement sand particles together and has emerged as a promising alternative to traditional ground-improvement treatments for granular soils. Owing to precipitation and absorption in different directions, MICP leads to anisotropic cementation. This study was aimed at examining the mechanism of cementation anisotropy and its treatment effect on two commonly used granular soils in geotechnical engineering: quartz sand and calcareous sand. A novel MICP technique was used to prepare bio-cemented sand specimens with different anisotropic patterns of cementation. Microscopic detection techniques were applied to examine the microstructure of the produced MICP cementation. The cementation in the vertical and horizontal directions was different, owing to gravity. The granular surface properties affected the content, morphology, and cement force of the bio-cements produced by MICP treatment. The results of unconfined compression strength experiments confirmed the occurrence of cementation anisotropy and its substantial effects on the stiffness, strength, and fracture patterns of MICP-treated quartz sand and calcareous sand. These findings can help to clarify the formation mechanism of bio-cements and promote the optimised application of MICP for the treatment of granular soils.

Keywords: Granular soils, Microbially induced calcium-carbonate precipitation, Cementation anisotropy, Treatment effect

1 Introduction

Microbially induced calcium-carbonate precipitation (MICP) has emerged as a promising alternative to traditional ground-improvement treatments [5, 12, 21, 30, 37, 44]. Ureolysis-driven MICP has attracted considerable interest as it can efficiently hydrolyse urea to carbonate ions, resulting in the rapid production of calcium carbonate crystals in a calcium source environment [4, 7]. The MICP process can be described as follows [15, 18, 33]:

$$CO(NH_2)_2 + 2H_2O \rightarrow 2NH_4^+ + CO_3^{2-} \quad (1)$$

$$Ca^{2+} + CO_3^{2-} \rightarrow CaCO_3(solid) \quad (2)$$

In recent years, MICP has been proven to be an effective bio-improvement method for granular soils, such as common quartz sand [2, 7, 9, 28-29, 32, 35, 46] and marine calcareous sand [10, 14, 22-24, 50, 53]. MICP can help enhance the physical and mechanical characteristics of both soil types, resulting in reduced settlement [11, 45], enhanced bearing capacity and liquefaction-resist foundations [6, 17, 30, 39, 43], decreased particle breakage [46, 53], and restrained seepage erosion [19, 25, 26]. Consequently, the mechanism of MICP and its treatment effect on granular soils has become a key area of research in recent years.

Precipitated cement crystals can bond soil particles together, thereby improving soil strength. The mechanical performance of MICP-treated soils is related to the microstructure of the MICP-associated cementation [4, 36]. The microstructure of MICP cementation is influenced by many factors, such as soil type [5], soil saturation [4, 38], solution concentration [1, 27, 42], and environmental conditions [6, 27, 47]. Particles of quartz sand have regular shapes and smooth surfaces [51]. Thus, MICP-produced cements coat the surfaces of particles, which leads to inter-particle bridging [9, 36] and generating cement-bonded sand particles that are the basis of effective MICP cementation [4, 9]. In contrast, calcareous sand particles are characterised by irregular morphologies and abundant intra-particle pores [8, 52], which can be filled by MICP treatment [53]. The effect of MICP-induced intra-particle pore filling on soil performance remains to be clarified.

Inherent material anisotropy is caused by loads such as gravity, wind, and waves during material deposition and is a key physical characteristic of natural sands [16]. Owing to this

anisotropy, soils exhibit distinct mechanical properties in different directions. Similarly, the MICP-induced production of crystals in a solution is influenced by gravity, owing to which anisotropic and heterogeneous cementation occurs within a soil matrix. MICP cementation anisotropy has been experimentally observed [36, 39-41, 48, 49] but its effects on soils have not been considered in laboratory settings or engineering applications, such as in reinforcement applications. That is, as foundation reinforcements are typically required to increase loading capacity and reduce settlement in the vertical direction, and breakwater and slope reinforcements are required to strengthen loading capacity in the horizontal direction, the treatment effect and mechanism of anisotropic cementation on the mechanical properties of MICP-treated granular soils in these contexts needs to be defined.

Therefore, this study was aimed at investigating the effects of soil type and cement anisotropy on the microstructures and mechanical behaviours of MICP-treated granular soils. Calcareous sand and quartz sand were divided into different groups in terms of deposition-load direction, treatment round, and grading. The microstructures of the produced bio-cements and their formation processes were investigated by scanning electron microscopy (SEM), X-ray diffraction (XRD), and Fourier-transform infrared spectroscopy (FTIR). Moreover, a particle-scale test was conducted to quantify the anisotropy and hydrophobicity of the MICP-produced cements under different treatment conditions. Finally, a series of unconfined compression strength (UCS) tests were conducted to clarify the impact of cementation anisotropy on the mechanical behaviours (i.e., strength, stiffness, and fracture patterns) of MICP-treated soil samples. The findings can help to clarify the effects and corresponding mechanisms of cementation anisotropy induced by MICP treatment on the soil behaviours of granular sands at different scales.

2 MICP treatment

Figure 1 shows the morphology of calcareous sand and quartz sand, which were collected from Spratly islands in the South China Sea and Fujian province, China, respectively. Two grading levels were selected: 0.5–1.0 mm and 1.0–2.0 mm. The calcareous sand consisted of biological remains (e.g., shells and corals) with angular shapes and abundant intra-particle

pores. In contrast, the quartz sand particles were characterised by rounded and smooth morphologies.

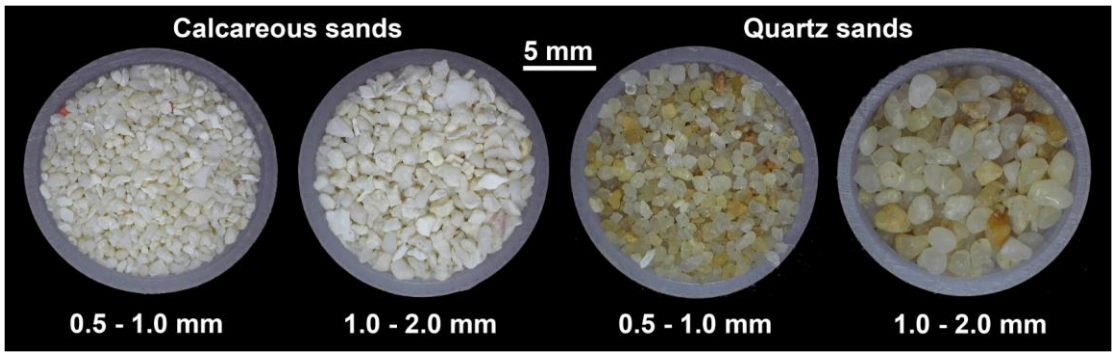

Fig. 1 Photographs of the tested calcareous sand and quartz sand

Sporosarcina pasteurii (ATCC 11859), a commonly used bacterium, was employed for MICP treatment. The bacterium was cultured at a temperature of 30 °C and pH of 8.5 in a liquid medium containing 20 g/L yeast extract (NH_4-YE), 10 g/L NH_4Cl, 12 mg/L $MnSO_4 \cdot H_2O$, and 24 mg/L $NiCl_2 \cdot 6H_2O$. The urease activity of the bacterial suspension (BS) was assessed by measuring its electrical conductivity after 24 h and was approximately 9.9–10.2 mM urea hydrolysed/min. The optical density at 600 nm (OD_{600}) of the BS was measured using an ultraviolet spectrophotometer and was 1.8–2.0. The cementation solution (CS) was composed of urea (CON_2H_4) and $CaCl_2$, with a concentration of approximately 0.5 mol/L after mixing [2].

Figure 2 illustrates the preparation of the MICP-treated sand specimens. A series of calcareous sand and quartz sand specimens with diameters of 38 mm and heights of 76 mm were prepared using a specially designed mould. The mould was created using a polyethylene bracket covered by a 2-mm-thick geotextile, which stabilised the uncemented sand particles while allowing the BS and CS to permeate the specimens. The specimens were designed to have different slope angles, resulting in anisotropic cementation with different precipitation directions. The two types of sand were divided into 30 groups that differed in terms of slope angle (0°, 45°, and 90°), grading (0.5–1.0 mm and 1.0–2.0 mm), and number of MICP treatment rounds (1–5). The relative density D_r of all of the specimens was controlled to approximately 0.62.

One round of MICP treatment involved the following three steps (1) Three parallel specimens were placed in a container and then treated with approximately 300 mL of the BS per specimen, such that the specimens were immersed. Subsequently, the container was placed in an incubator and heated at 30 °C for 24 h. (2) The specimens were transferred to a new empty container in the incubator and then treated with 500 mL per specimen of the CS to trigger carbonate precipitation, and the specimens were heated at 30 °C for 24 h. (3) Repeating step two. Thus, overall, the specimens were immersed in the BS for 24 h and then in the CS for 48 h for one round of MICP treatment. After the MICP treatment, the geotextile covers on the specimens were removed, the MICP-treated sand specimens were washed with deionised water and then dried at 60 °C for 24 h.

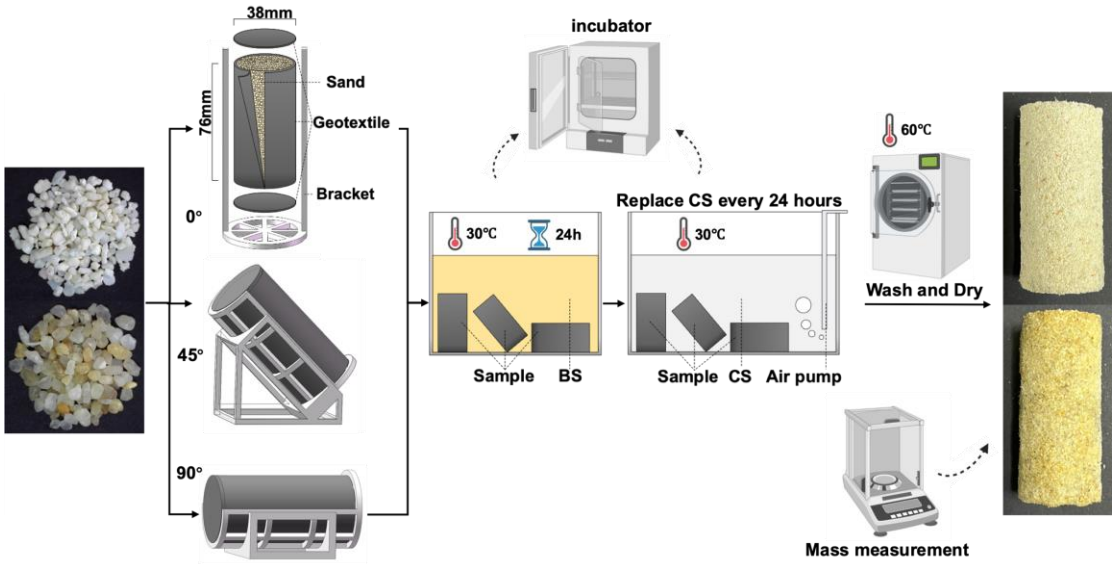

Fig. 2 MICP treatment processes

3 Precipitation mechanisms of bio-cements

3.1 Evolution of the bio-cement content

The bio-cement content *C* is a key indicator of the treatment effect of MICP. Acid washing is typically used to measure the bio-cement content of MICP-treated quartz sand specimens [1, 10]. However, calcareous sand particles, which are mainly composed of calcium carbonate, may be easily corroded by acid washing. Therefore, in this study, the *C* values of MICP-treated quartz sand and calcareous sand specimens were determined as follows:

$$C = \frac{M_1 - M_0}{M_0} \times 100\% \quad (3)$$

where M_0 and M_1 are the dried weights of a specimen before and after MICP treatment, respectively.

Figure 3 shows the variation of C with the number of MICP treatment rounds. In all specimens, C rapidly increased in the initial rounds of treatment and then plateaued. The latter occurred because the filling of inter-particle voids by the MICP-produced cements inhibited the biochemical processes involved in MICP. Additionally, the C values of the MICP-treated calcareous sand specimens were approximately twice those of the MICP-treated quartz sand specimens. Specimens of both types of sands with a fine grading had a lower C than those with the coarse grading. These results demonstrated that the high specific surface area of the soil matrix associated with the fine particles or the presence of intra-particle voids promoted MICP, thereby achieving a better MICP treatment effect than was possible in a soil matrix associated with coarse particles.

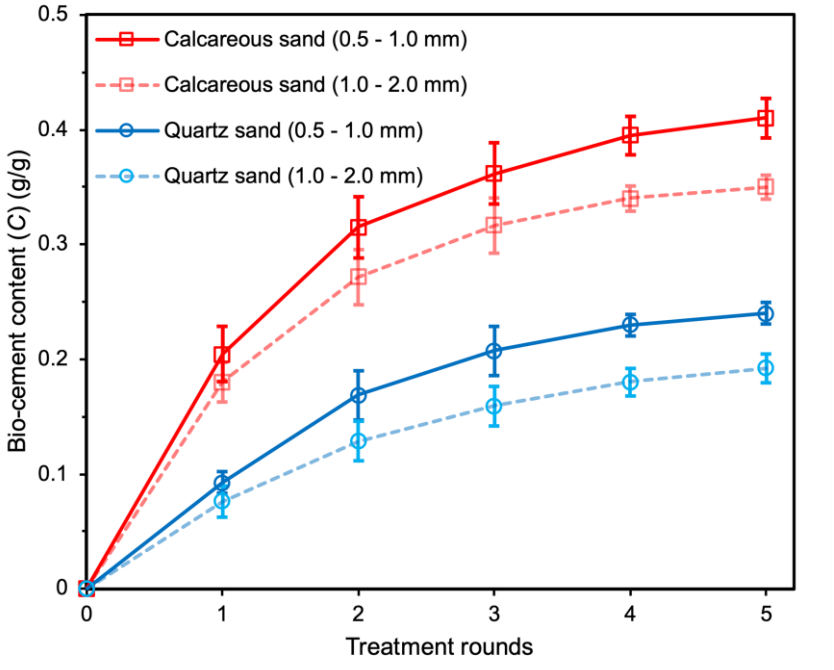

Fig. 3 Development of the bio-cement content with the number of MICP treatment rounds

3.2 Microstructural characteristics

XRD and FTIR spectroscopic analyses were performed to examine the composition and

microstructure of the MICP-produced bio-cements. Given that the calcareous sand and bio-cements were composed of calcium carbonate, three specimens (untreated calcareous sand, treated calcareous sand, and treated quartz sand) were separately ground into powder for mineral phase identification by XRD spectroscopic analysis. Figure 4 shows the XRD results; as expected, the mineral components of the calcareous sand, quartz sand, and bio-cement were aragonite, quartz, and calcite, respectively.

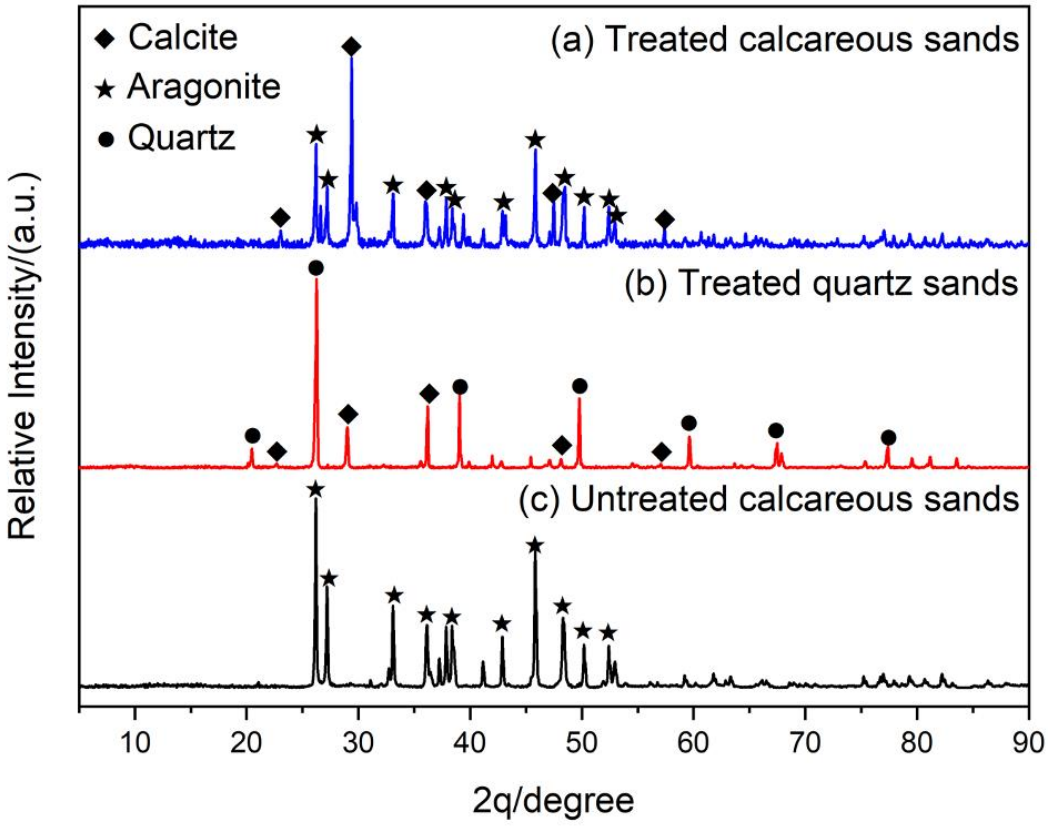

Fig. 4 Phase identification of the materials through XRD

Specimens for FTIR spectroscopic analysis were prepared by separately grinding untreated and MICP-treated calcareous sand and quartz sand into powder and subjecting these to water-removal treatment. Figure 5 shows the FTIR spectra of the calcareous sand and quartz sand specimens before and after MICP treatment. The chemical bonds possibly represented by peaks were determined by reference to reported infrared absorption band frequencies [3, 20, 31]. C=O and C–O peaks were detected in the untreated calcareous sand specimens, whereas Si–O–Si and O–Si–O peaks were detected in the untreated quartz sand specimens. Additionally, O–H

peaks were observed at approximately 1600 cm^{-1} and 710 cm^{-1}, owing to the generation of hydroxyl groups on the silica surface exposed to air for a considerable period [31, 34]. C=O and C–O peaks were observed in the MICP-treated quartz sand specimens. A new O–H peak was observed at approximately 3430 cm^{-1}, and another new O–H peak overlapped with the old O–H peak at 710 cm^{-1} to enhance the absorption peak.

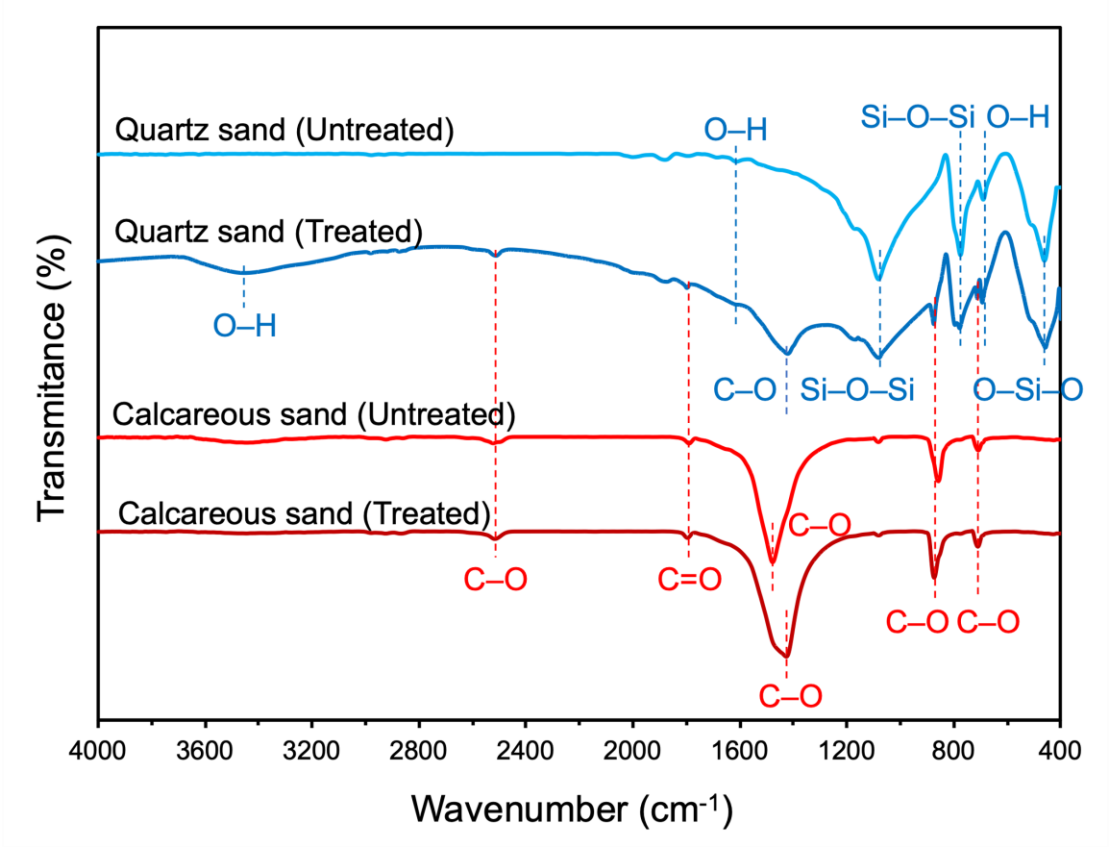

Fig. 5 FTIR spectra of the tested materials

The FTIR spectroscopic analysis results indicated that the hydroxyl groups on the surface of quartz sand particles formed hydrogen bonds with the oxygen atoms of the bio-cement. In contrast, only van der Waals forces – which are weaker than hydrogen bonds – were generated between the calcareous sand and bio-cement. Figure 6 illustrates the why these different intermolecular forces arose in the different types of bio-cemented sand. When the surface of quartz sand was exposed to air for a considerable period, hydroxyl groups were generated on silica that combined with the oxygen atoms of the bio-cement to form hydrogen bonds. In contrast, calcareous sand is composed of calcium carbonate, which is an alkaline salt. Therefore,

no hydroxyl groups were produced on the surface, and only van der Waals' forces were generated between the particle surface and bio-cement.

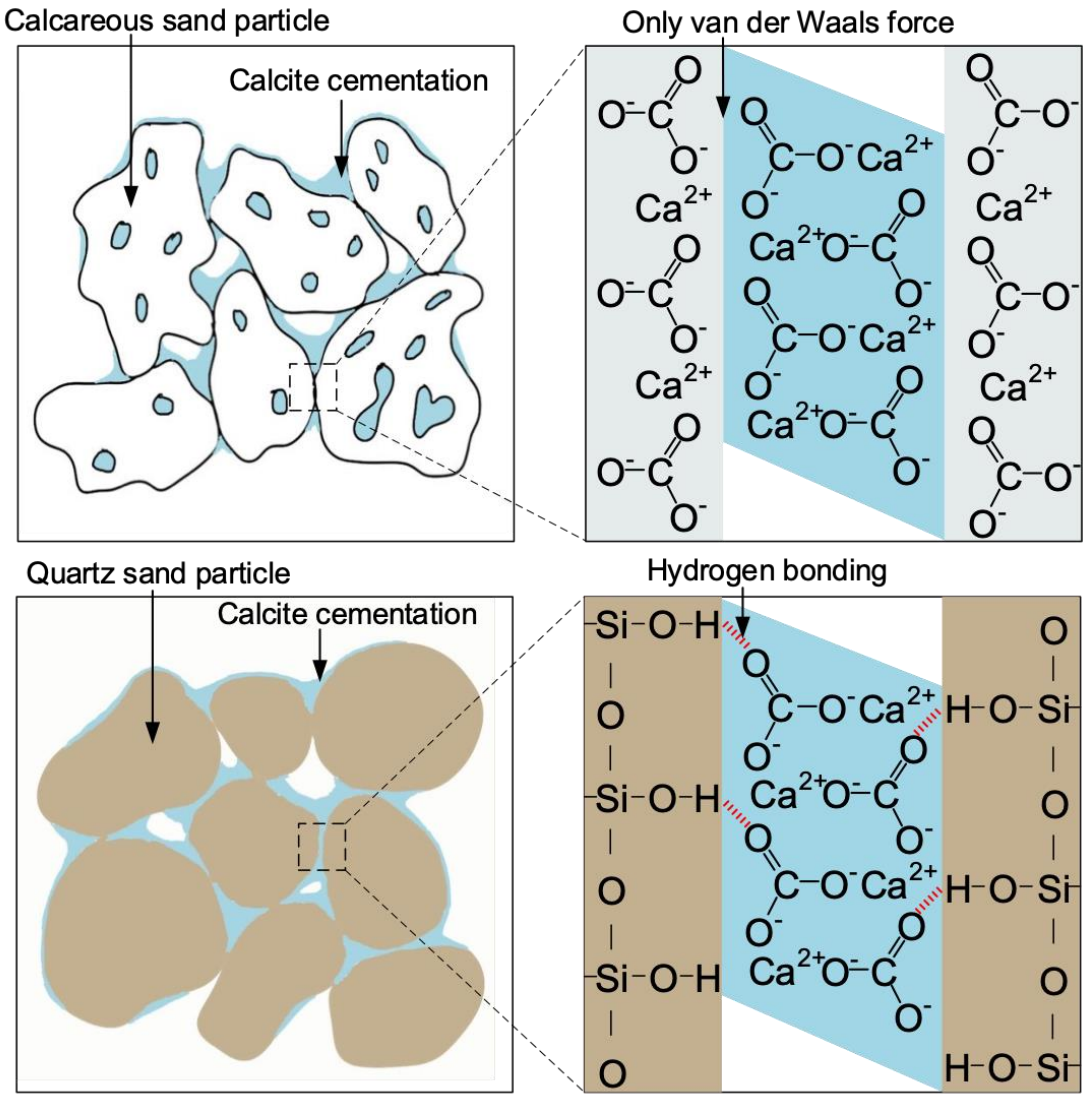

Fig. 6 Schematic of intermolecular forces between MICP-produced bio-cements and original particle composition for calcareous sand and quartz sand.

To investigate the cementation anisotropy induced by MICP, cubic (length = 8 mm) specimens of the MICP-treated sands were manufactured. SEM scanning was performed in the horizontal and vertical directions of each cubic specimen to examine bio-cement distributions, as shown in Fig. 7. The horizontal (red face) and vertical (blue face) directions of the cubic specimens were defined to be perpendicular to and parallel to the direction of gravity,

respectively. Figure 8 shows SEM images of the untreated and MICP-treated specimens. The particle surfaces of the treated calcareous sand were fully coated with uniformly and densely distributed calcite crystals, whereas the particle surfaces of the treated quartz sand were partially coated with sparsely distributed calcite agglomerates. The calcite crystals of the calcareous sand were polyhedral, whereas those of the quartz sand were spheroidal. These results indicate that the rich intra-particle pores within calcareous sand were conducive to bacterial adsorption and calcite crystallisation during the MICP treatment.

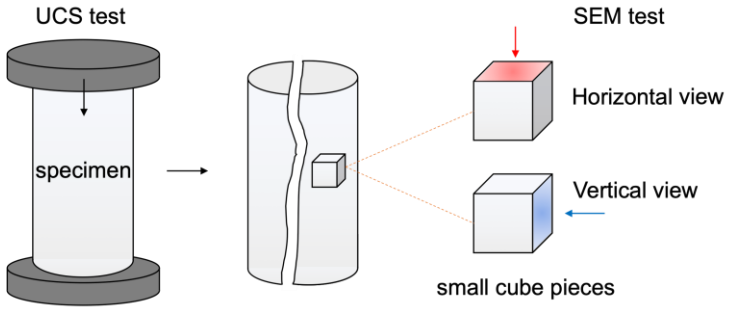

Fig. 7 Sample preparation for SEM observation

Based on the microstructural characteristics of the bio-cements, the treatment mechanisms for calcareous sand and quartz sand were derived, as shown in Fig. 9. In the case of calcareous sand, MICP led to global particle-surface coating, inter-particle contact bridging, and intra-particle pore filling. In contrast, in the case of quartz sand, MICP resulted only in inter-particle bridging and local particle-surface accumulation. Owing to the rapid and extensive calcite production associated with global particle-surface coating and intra-particle pore filling, the *C* value of the calcareous sand increased more rapidly than that of the quartz sand, especially in the earlier rounds of MICP treatment (Fig. 4). This result was consistent with the findings of the authors' previous study, in which MICP treatment was applied to individual calcareous sand particles [53].

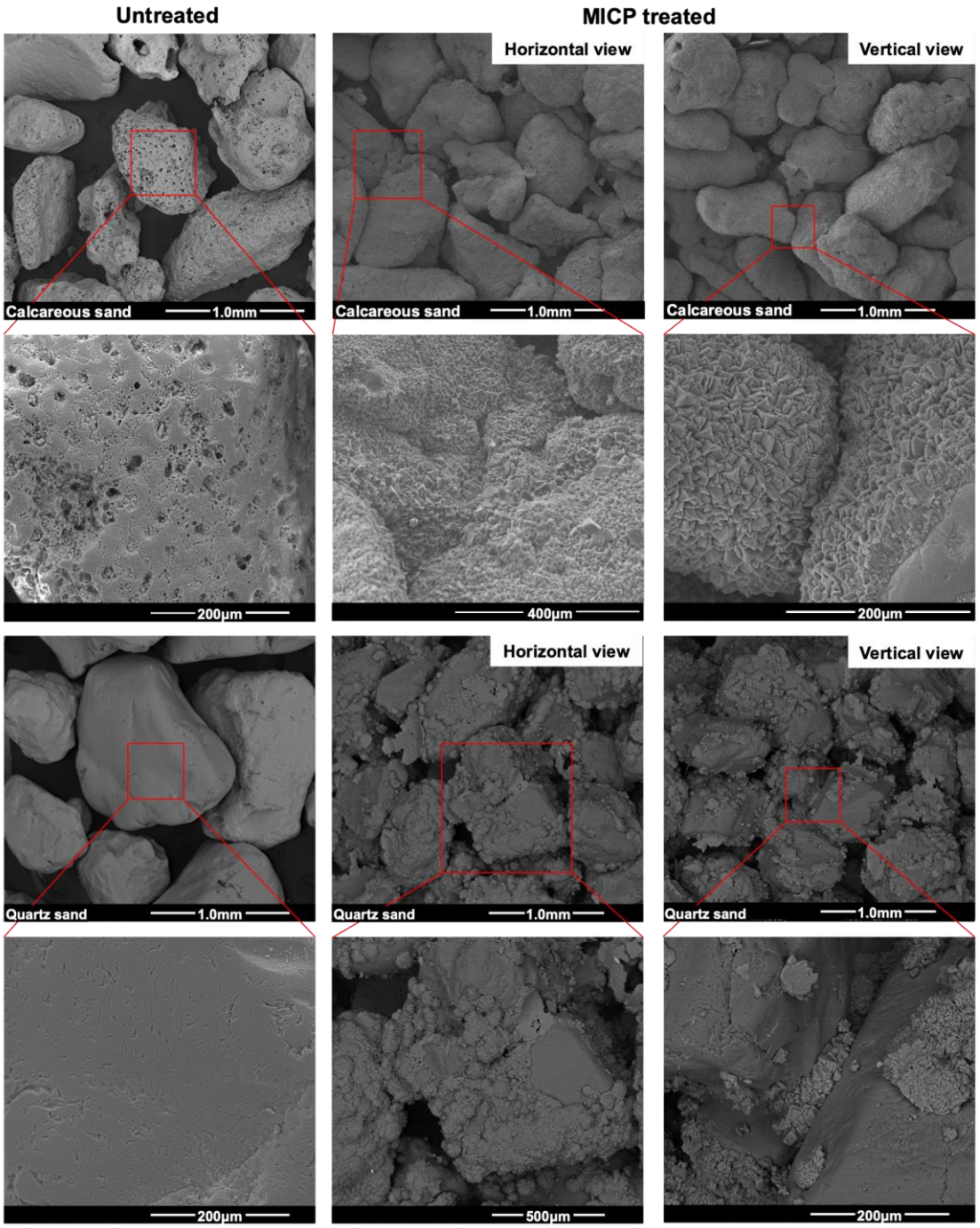

Fig. 8 SEM images of the calcareous sand and quartz sand specimens. The first, second, and third columns correspond to untreated specimens, MICP-treated specimens (horizontal view), and MICP-treated specimens (vertical view), respectively.

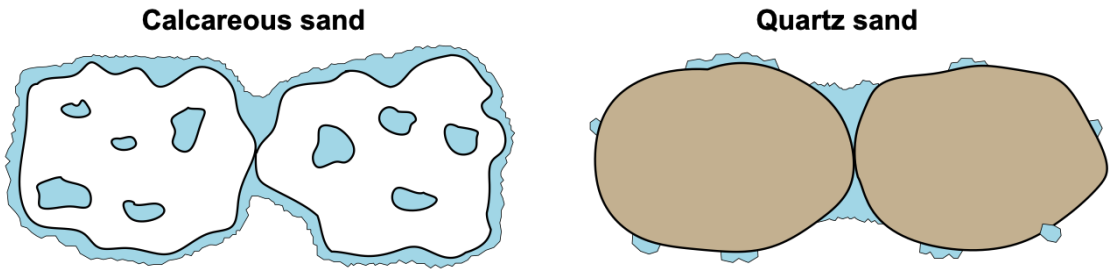

Fig. 9 MICP-treatment mechanisms for calcareous sand and quartz sand.

3.3 Origin of bio-cement anisotropy

The SEM images in Fig. 8 show that the distribution densities of the MICP-produced bio-cements varied with direction, especially in the quartz sand. Thus, a particle-scale test was conducted to quantify the cementation anisotropy induced by MICP. Figure 10 illustrates the workflow of the test. First, standard cubes with lengths of 10 mm were manufactured using individual quartz and calcareous gravel particles. These cubes were then individually treated via the MICP process described in Section 2, with the cubes being suspended in the BS or CS using plastic clips and with appropriate surfaces of the cubes covered with waterproof tape strips to leave only a target surface or surfaces free for MICP. Subsequently, the *C* values of the bio-cements produced on the target surface(s), i.e., the top surface, the side surfaces, and the bottom surface, were measured. To obtain measurements for the top surface, for example, the side and bottom surfaces of a cube were covered before MICP treatment. The *C* value on the top surface was directly measured by removing these tapes after MICP treatment due to bio-cement coating on the tape.

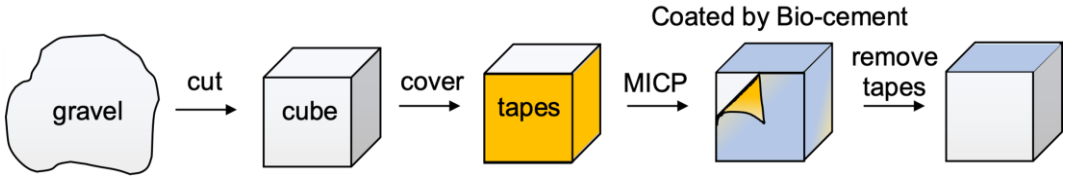

Fig. 10 Process flow of the cube test.

Figure 11 shows the surface morphologies of the cubes before and after MICP treatment. The top and bottom surfaces, which faced toward and away from gravity, presented the thickest and thinnest bio-cement coating layers, respectively. The surface coating thicknesses increased

with as the number of treatment rounds increase.

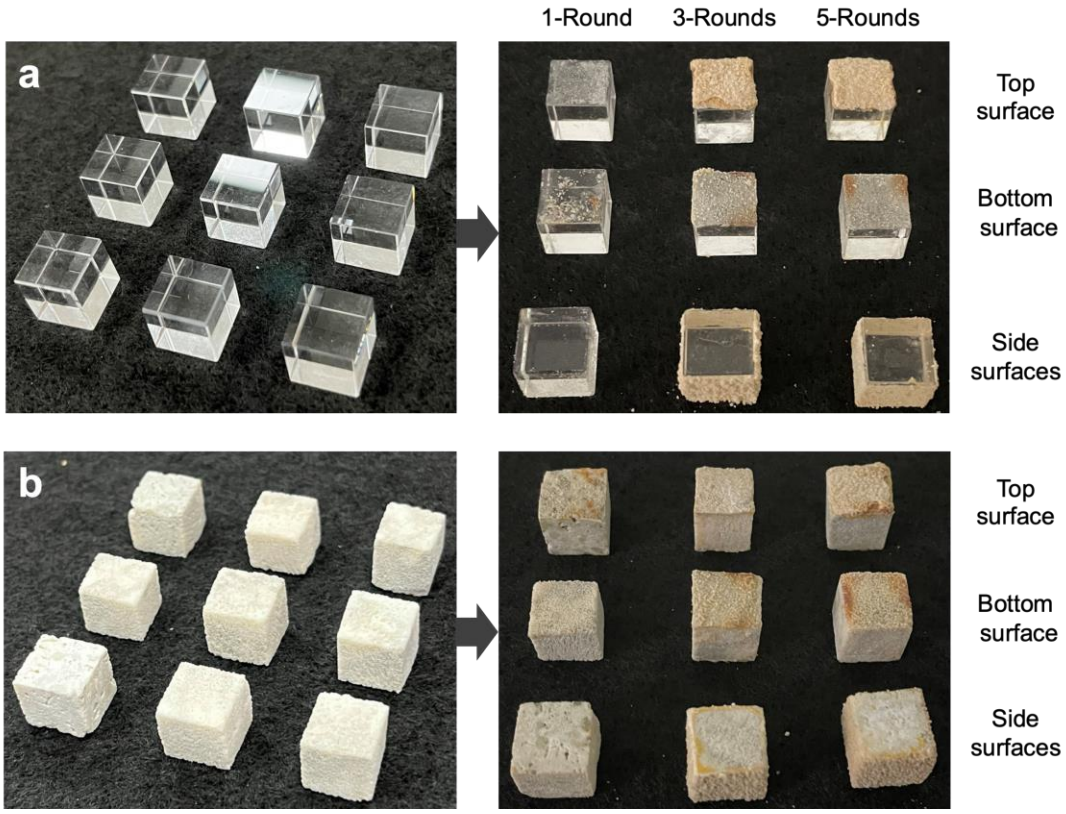

Fig. 11 Morphologies of (a) quartz and (b) calcareous cubes before and after MICP treatment

Figure 12 shows the variation in the *C* values for various cube faces with increasing numbers of treatment rounds. The top surface exhibited the largest proportion of bio-cements produced during MICP (70% and 60% for quartz sand and calcareous sand, respectively). This indicates that the MICP treatment of both sands resulted in significant cementation anisotropy. The *C* values of the side surfaces were slightly larger than those for the bottom surface. The production of bio-cements on the bottom surface indicated the significant surface-adsorption effect of the particles, which not only contributed to the formation of bio-cement microstructures but also helped overcome the restraining effect of gravity on the MICP process. That is, surface adsorption resulted in the adsorption of bacteria and the aggregation of calcite crystals dispersed in solution.

The degree of anisotropy of the MICP-produced bio-cements increased as the number of treatment rounds increased. This is attributable to the variation in the surface adsorption induced by the surface covering of the bio-cements. In general, adsorption is strongly correlated with the surface hydrophilicity of materials. To examine the variation in the adsorption effect

during MICP, a static water contact angle test was conducted. Specifically, a 5 μL droplet of deionised water was placed on the surface of the cubic specimens, and the contact angle between the droplet and the surface was measured after 5 s. The final result was the average of five measurements recorded at different locations on the cube surface.

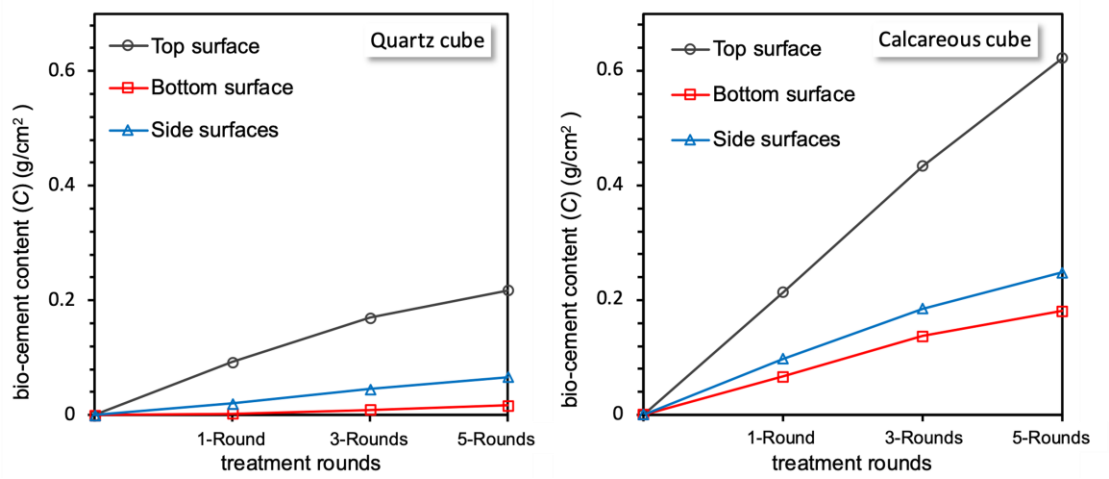

Fig. 12 Evolution of *C* values on various surfaces with number of treatment rounds

Figure 13 shows the water contact angles on the cubes before and after MICP treatment. The water contact angles of the untreated calcareous cube and quartz cube were small, due to the strong hydrophilicity of the natural quartz sand and calcareous sand. As the number of treatment rounds increased, the water contact angles on all of the surfaces of both types of sands gradually increased. This indicates that the growth of the calcite cements decreased surface hydrophilicity, i.e., the surface adsorption, of both types of sand particles, consistent with the results of recent studies [13, 25]. This decline in surface adsorption decreased the rate of increase of the *C* value (Fig. 3) and enhanced the anisotropy of the bio-cements generated in both types of MICP-treated sands.

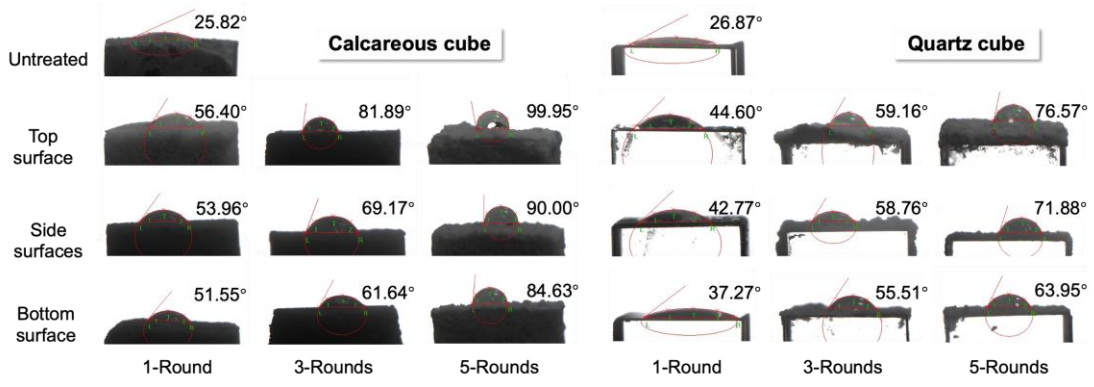

Fig. 13 Static water contact angles of the cubes before and after MICP treatment

4 Anisotropy of Mechanical Behaviour

4.1 Stress–strain behaviour

Figure 14 shows that bio-cement formation led to horizontal delamination of the microstructure, owing to gravity effects during MICP treatment and surface absorption changes generated by MICP treatment. To investigate the effect of the bio-cement anisotropy on the mechanical behaviours of the MICP-treated samples, UCS tests were performed. A constant loading rate of 0.1 mm/s was applied to uniaxially compress the sand specimens until failure, with the angles between the deposition direction with respect to gravity during MICP treatment and the loading direction during the UCS test set to 0°, 45°, and 90°.

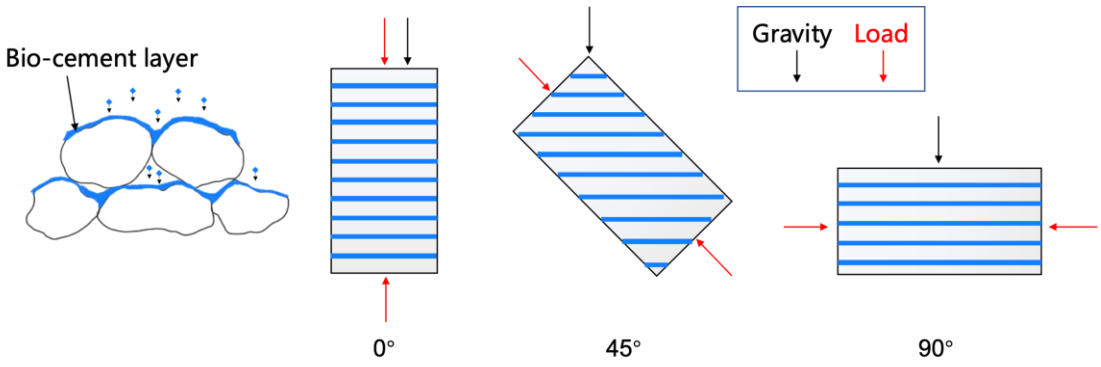

Fig. 14 Anisotropy of mechanical properties owing to bio-cement deposition

Figure 15 shows the stress–strain curves obtained from the UCS tests of sand specimens subjected to MICP treatments differing in terms of the number of rounds (1, 3, and 5) and deposition direction. A shear failure mode similar to that of sandstone was observed. With an increase in the number of treatment rounds and in the deposition-load angle, the UCS gradually increased, and the probability of brittle failure increased. However, stress softening occurred after the sand specimens yielded under compression in a one-round treatment with a small deposition-load angle. After the UCS of the specimens with a deposition-load angle of 90° reached its maximum value, it sharply decreased, representing a typical brittle-fracture mode.

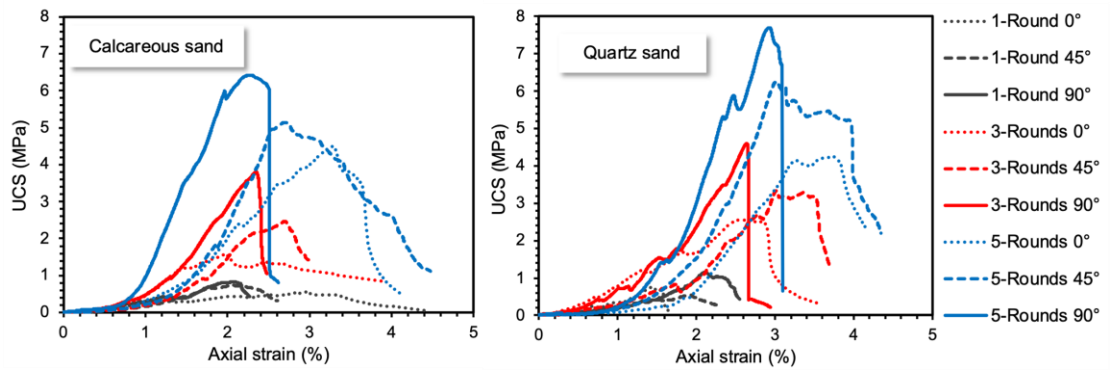

Fig. 15 Typical stress–strain curves obtained from the UCS tests of (a) calcareous sand and (b) quartz sand with particle sizes of 0.5–1.0 mm

4.2 Strength and stiffness

Strength and stiffness are two commonly used indicators and were chosen to quantify the mechanical behaviour of the bio-cemented sands. Strength was defined as the maximum peak stress in the stress–strain curve shown in Fig. 15. Stiffness was defined as the tangent modulus at 50% of the peak stress, E_{50}, and it was determined from the stress–strain curve [23, 37].

Figures 16 and 17 show the strength–C and stiffness–C curves at different deposition-load angles, respectively. In calcareous sand, the proportion of effective cementation – which is the key factor determining the compressive strength of bio-cemented specimens – was small in the early stage of MICP treatment. The cementation proportion gradually increased as the intra-particle pores were filled and the surfaces were completely coated. The UCS–C and E_{50}–C relationships of the bio-cemented calcareous sand were expected to be nonlinear. Therefore, a power function was used to depict the fitting curve. In quartz sand, it was expected that the proportion of effective cementation would be constant during the MICP treatment, as the coating and filling effects in this sand were weak. Therefore, a linear function was used to describe the UCS–C and E_{50}–C relationships of this sand. When the bio-cement contents of calcareous sand and quartz sand reached approximately 15% and 7%, the UCS and E_{50} of both types of sand approached 0.5 MPa and 25 MPa, respectively. This indicates that the strength and stiffness were activated at C values of approximately 10% and 5% for calcareous sand and quartz sand, respectively. Thus, complete covering of particle surfaces and filling of intra-particle pores did not enhance the cohesion of the sand matrix.

All of the specimens exhibited anisotropic mechanical behaviours regardless of particle size, and the degree of anisotropy increased with the *C* value. Specifically, the strength and stiffness values of the specimens were maximised and minimised when the deposition-load angles were 90° and 0°, respectively. This indicates that horizontal delamination of the bio-cement microstructures resulted in anisotropic mechanical behaviours. Specifically, compression in the directions of dense and sparse bio-cementation resulted in higher and lower strengths, respectively.

At the maximum *C* values, the strengths of the two types of bio-cemented sands were similar. In contrast, the stiffness of the bio-cemented quartz sand was slightly lower than that of the bio-cemented calcareous sand. These results can be explained as follows. First, the hydroxyl groups on the surface of the quartz sand particles formed hydrogen bonds with the oxygen atoms of the bio-cement that were stronger than the van der Waals' force generated between the calcareous sand and the bio-cement. However, the higher bio-cement content of calcareous sand overcame the deficiency of its intermolecular forces, such that it had similar strength to the bio-cemented quartz sand. Second, the irregular morphology enhanced the self-locking effect of the inter-particles of the bio-cemented calcareous sand, which enhanced its stiffness.

The UCS and E_{50} values of the bio-cemented calcareous sand specimens with the grading of 0.5–1.0 mm were 0.4–6.5 MPa and 20–550 MPa, respectively, and those of the same grading of bio-cemented quartz sand were 0.5–8.5 MPa and 50–500 MPa, respectively. The UCS and E_{50} values of the bio-cemented calcareous sand specimens with the grading of 1.0–2.0 mm were 0.3–4.5 MPa and 20–420 MPa, respectively, and those of the same grading of bio-cemented quartz sand were 0.5–6.8 MPa and 20–420 MPa, respectively. At a given *C* value, specimens of each type of sands with finer gradings exhibited higher UCS values than those with coarser gradings, although the stiffness values of different gradings of each type of sand were similar. This, the compressive stiffness of the specimens was related to only the *C* value and not the grading.

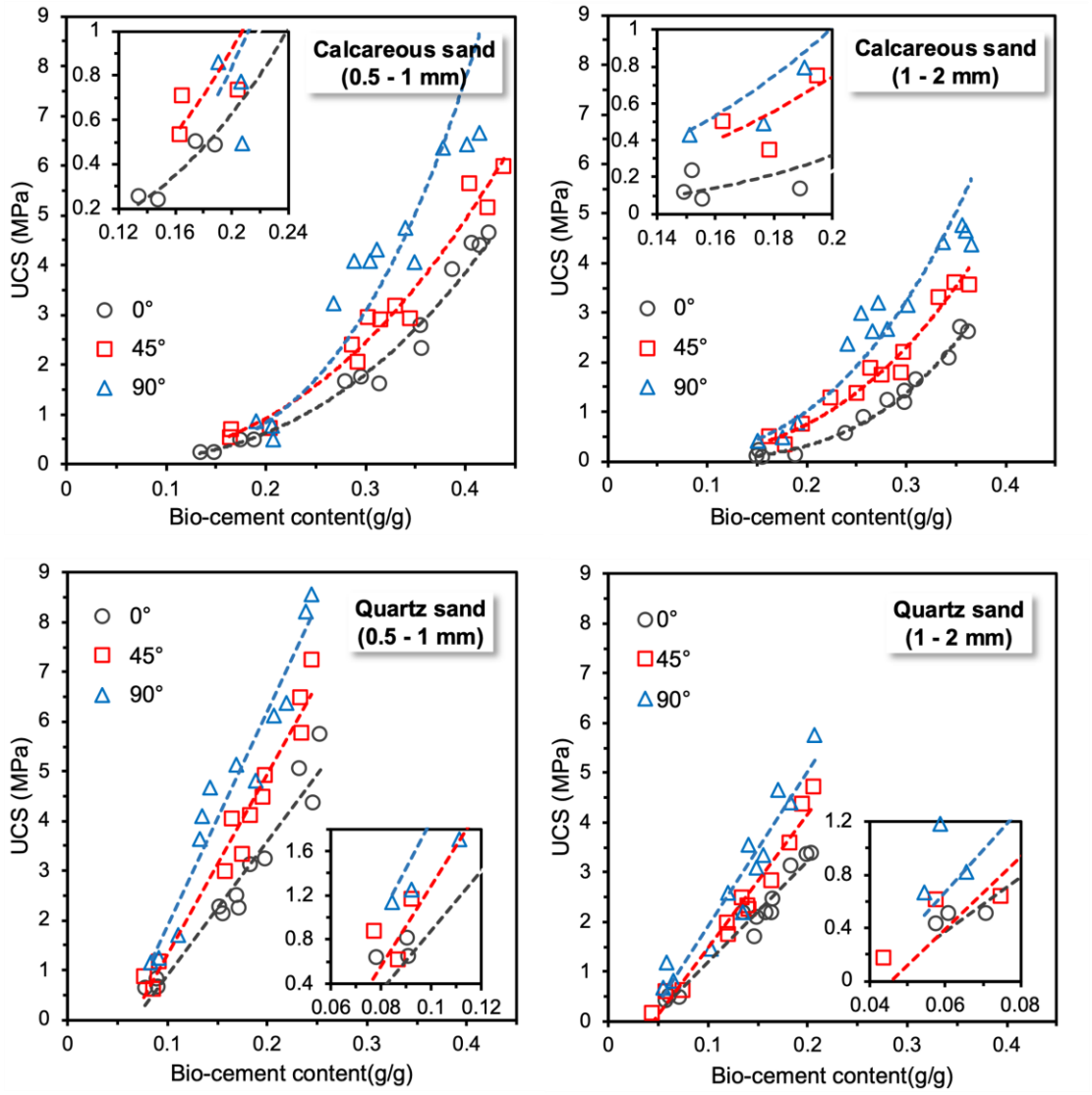

Fig. 16 Relationship between the unconfined compression strength (UCS) and bio-cement content

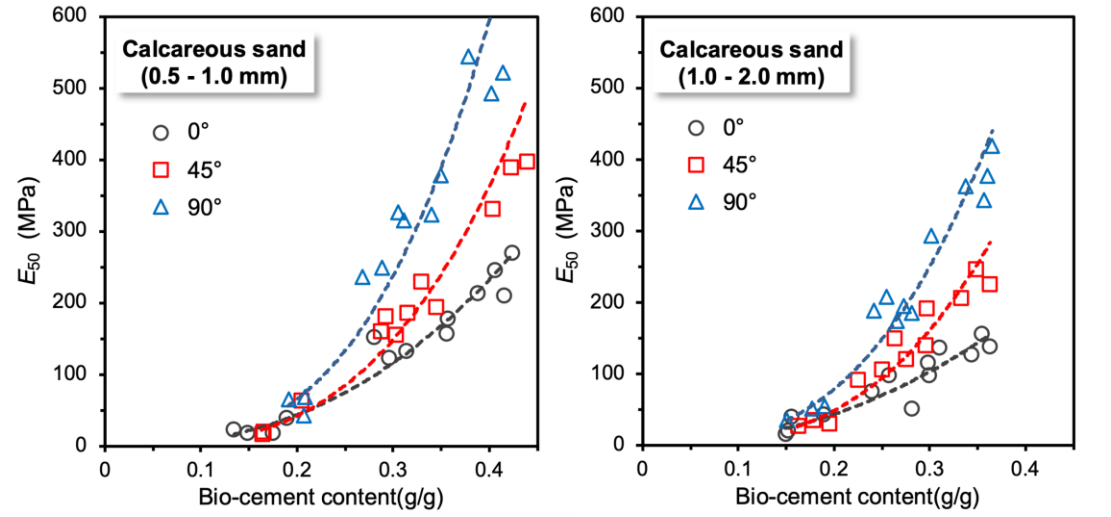

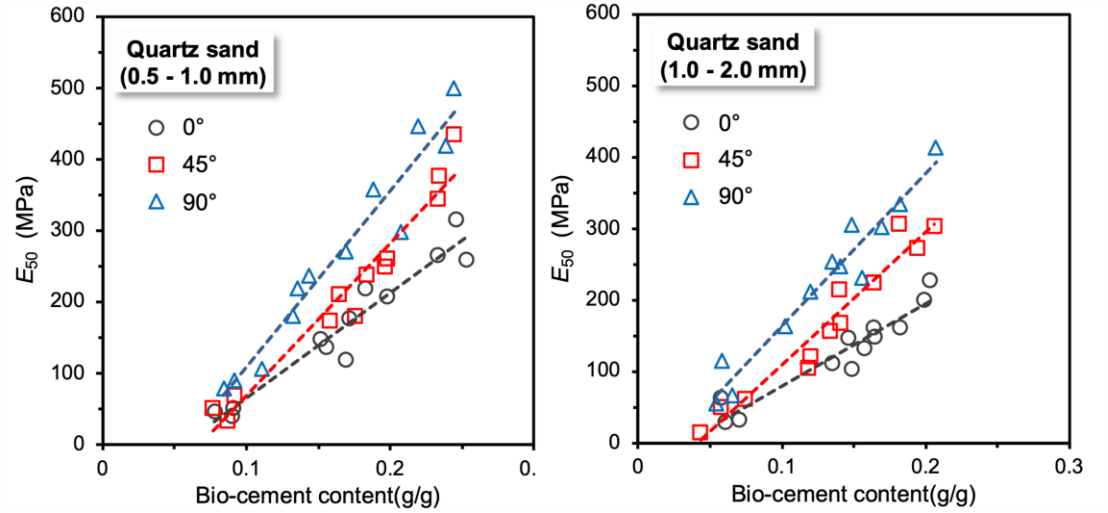

Fig. 17 Relationship between E_{50} and bio-cement content

4.3 Fracture pattern

In the UCS tests, regular fracture patterns were observed in the specimens subjected to five treatment rounds, and sand specimens with different particle sizes exhibited similar fracture patterns. Therefore, the variation in the failure patterns with the deposition direction was examined, as shown in Fig. 18. Shear bands and cracks (marked in red in the figure) appeared in the specimens. Specifically, corner chopping was observed in specimens with a deposition-load angle of 0°, and these specimens contained no regular shear bands. Regular 45° shear bands were present in the specimens with a deposition-load angle of 45°. Shear bands spanned the entire length of the specimens with a deposition-load angle of 90°. Thus, the direction of shear banding was strongly correlated with the deposition-load angle. Moreover, the bio-cemented specimens underwent brittle failure; cracks developed along the layer of the bio-cement microstructure, as the bonds were the weakest between layers.

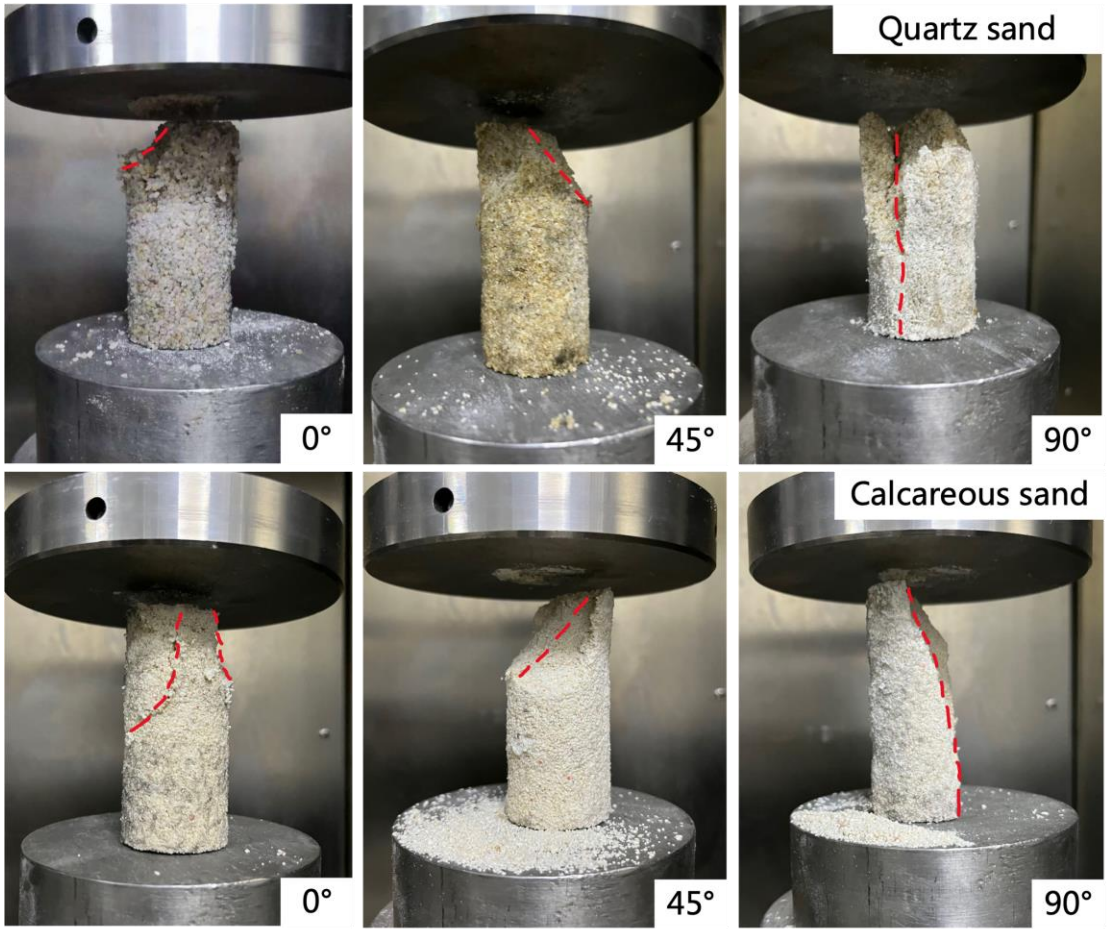

Fig. 18 Failure patterns of bio-cement sand specimens with different deposition directions

5 Conclusions

The cementation anisotropy induced by MICP and its effects on the mechanical properties of treated quartz sand and calcareous sand were comprehensively investigated. MICP was used to prepare bio-cemented sand specimens with different anisotropic patterns of cementation. Microscopic analyses were used to evaluate the microstructures of the produced bio-cements. UCS tests were conducted to clarify the influence of cementation anisotropy on the stiffness, strength, and fracture patterns of both types of granular sands subjected to MICP treatment. The following conclusions were derived.

(1) In comparison to quartz sand, the abundant intra-particle pores and surface holes of calcareous sand promoted bacterial adsorption and calcite precipitation during MICP, resulting in the production of a larger amount of bio-cement in the same biochemical environment. MICP led to global particle-surface coating, inter-particle contact bridging, and intra-particle pore

filling in calcareous sand, but only local particle-surface covering and inter-particle bridging in quartz sand. However, the intermolecular forces of the bio-cement acting on quartz particle surfaces (hydrogen bonds) were considerably stronger than those of the bio-cement acting on calcareous sand particle surfaces (van der Waals' forces).

(2) MICP induced significant cementation anisotropy over the real sand specimens and the cubic specimens. After MICP, the top surface of each cubic specimen (i.e., the surface facing the direction of gravity) exhibited a *C* value that was higher than those exhibited by the side and bottom surfaces. The natural quartz sand and calcareous sand particles exhibited strong surface hydrophilicity. However, this hydrophilicity was weakened by the growth of the MICP-produced calcite cements, owing to intermolecular interactions and closure of intra-particle and inter-particle pores. Therefore, the degree of anisotropy of the bio-cements formed on both types of sands intensified with the number of rounds of MICP treatment.

(3) Both MICP-treated sands exhibited similar UCS values, owing to the moderating effects of the higher *C* of calcareous sand and the stronger intermolecular forces within quartz sand. Owing to the stronger inter-locking between irregular particles in the MICP-treated calcareous sand, it exhibited a higher compressive stiffness than the MICP-treated quartz sand. Horizontal layers of bio-cements were generated, owing to the effects of gravity and particle surface adsorption during MICP. Consequently, the compressive strengths and stiffnesses of the MICP-treated sands were anisotropic. The lowest and highest compressive strengths and stiffnesses for each specimen occurred in the directions parallel and perpendicular to gravity, respectively.

Acknowledgments

This study was supported by Research Grants 42072298 and 41931286 from the National Natural Science Foundation of China.

References

1. A. Al Qabany, K. Soga, C. Santamarina, Factors affecting efficiency of microbially induced calcite precipitation, Journal of Geotechnical and Geoenvironmental Engineering 138(8) (2012) 992-1001. https://doi.org/10.1061/(ASCE)GT.1943-5606.0000666

2. A. Al Qabany, K. Soga, Effect of chemical treatment used in MICP on engineering properties of cemented soils. In Bio-and Chemo-Mechanical Processes in Geotechnical Engineering: Géotechnique Symposium in Print (2013) 107-115. https://doi.org/10.1680/bcmpge.60531.01f0.

3. G. Anbalagan, A. Prabakaran, S. Gunasekaran, Spectroscopic characterization of Indian standard sand, Journal of applied spectroscopy 77 (2010) 86-94. https://doi.org/10.1007/s10812-010-9297-5.

4. L. Cheng, R. Cord-Ruwisch, M.A. Shahin, Cementation of sand soil by microbially induced calcite precipitation at various degrees of saturation, Canadian Geotechnical Journal 50(1) (2013) 81-90. https://doi.org/10.1139/cgj-2012-0023

5. L. Cheng, M. Shahin, R. Cord-Ruwisch, Bio-cementation of sandy soil using microbially induced carbonate precipitation for marine environments, Géotechnique 64(12) (2014) 1010-1013. https://doi.org/10.1680/geot.14.T.025.

6. L. Cheng, M.A. Shahin, D. Mujah, Influence of key environmental conditions on microbially induced cementation for soil stabilization, Journal of Geotechnical and Geoenvironmental Engineering 143(1) (2017) 04016083. https://doi.org/10.1061/(ASCE)GT.1943-5606.0001586.

7. J. Chu, V. Ivanov, M. Naeimi, V. Stabnikov, H.-L. Liu, Optimization of calcium-based bioclogging and biocementation of sand, Acta Geotechnica 9 (2014) 277-285. https://doi.org/10.1007/s11440-013-0278-8.

8. M. Coop, The mechanics of uncemented carbonate sands, Géotechnique 40(4) (1990) 607-626. https://doi.org/10.1680/geot.1990.40.4.607.

9. M.-J. Cui, J.-J. Zheng, R.-J. Zhang, H.-J. Lai, J. Zhang, Influence of cementation level on the strength behaviour of bio-cemented sand, Acta Geotechnica 12 (2017) 971-986. https://doi.org/10.1007/s11440-017-0574-9.

10. M.-J. Cui, J.-J. Zheng, J. Chu, C.-C. Wu, H.-J. Lai, Bio-mediated calcium carbonate precipitation and its effect on the shear behaviour of calcareous sand, Acta Geotechnica 16 (2021) 1377-1389. https://doi.org/10.1007/s11440-020-01099-0.

11. J.T. DeJong, M.B. Fritzges, K. Nüsslein, Microbially induced cementation to control sand response to undrained shear, Journal of geotechnical and geoenvironmental engineering 132(11) (2006) 1381-1392. https://doi.org/10.1061/(ASCE)1090-0241(2006)132:11(1381).

12. J. DeJong, K. Soga, E. Kavazanjian, S. Burns, L. Van Paassen, A. Al Qabany, A. Aydilek, S. Bang, M. Burbank, L.F. Caslake, Biogeochemical processes and geotechnical applications: progress, opportunities and challenges, Bio-and chemo-mechanical processes in geotechnical engineering: géotechnique symposium in print 2013, Ice Publishing, 2014, pp. 143-157. https://doi.org/10.1680/bcmpge.60531.014.

13. H.A. Dovom, A.M. Moghaddam, M. Karrabi, B. Shahnavaz, Improving the resistance to moisture damage of cold mix asphalt modified by eco-friendly Microbial Carbonate Precipitation (MCP), Construction and Building Materials 213 (2017) 131-141. https://doi.org/10.1016/j.conbuildmat.2019.03.262.

14. M. Dyer, M. Viganotti, Oligotrophic and eutrophic MICP treatment for silica and carbonate sands, Bioinspired, Biomimetic and Nanobiomaterials 6(3) (2016) 168-183. https://doi.org/10.1680/jbibn.16.00002.

15. S. Goodarzi, H. Shahnazari, Strength enhancement of geotextile-reinforced carbonate sand, Geotextiles and Geomembranes 47(2) (2019) 128-139. https://doi.org/10.1016/j.geotexmem.2018.12.004.

16. N. Guo, L. Chen, Z. Yang, Multiscale modelling and analysis of footing resting on an anisotropic sand, Géotechnique 72(4) (2022) 364-376. https://doi.org/10.1680/jgeot.20.P.306.

17. J. He, J. Chu, Undrained responses of microbially desaturated sand under monotonic loading, Journal of Geotechnical and Geoenvironmental Engineering 140(5) (2014) 04014003. https://doi.org/10.1061/(ASCE)GT.1943-5606.0001082.

18. M.A. Ismail, H.A. Joer, W.H. Sim, M.F. Randolph, Effect of cement type on shear behavior of cemented calcareous soil, Journal of geotechnical and geoenvironmental engineering 128(6) (2002) 520-529. https://doi.org/10.1061/(ASCE)1090-0241(2002)128:6(520).

19. N.-J. Jiang, C.-S. Tang, L.-Y. Yin, Y.-H. Xie, B. Shi, Applicability of microbial calcification method for sandy-slope surface erosion control, Journal of Materials in Civil Engineering 31(11) (2019) 04019250. https://doi.org/10.1061/(ASCE)MT.1943-5533.0002897.

20. A.K. Kronenberg, H.F. Hasnan, C.W. Holyoke III, R.D. Law, Z. Liu, J.B. Thomas, Synchrotron FTIR imaging of OH in quartz mylonites, Solid Earth 8(5) (2017) 1025-1045. https://doi.org/10.5194/se-8-1025-2017.

21. K.-W. Liu, N.-J. Jiang, J.-D. Qin, Y.-J. Wang, C.-S. Tang, X.-L. Han, An experimental study of mitigating coastal sand dune erosion by microbial-and enzymatic-induced carbonate precipitation, Acta Geotechnica 16 (2021) 467-480. https://doi.org/10.1007/s11440-020-01046-z.

22. L. Liu, H. Liu, Y. Xiao, J. Chu, P. Xiao, Y. Wang, Biocementation of calcareous sand using soluble calcium derived from calcareous sand, Bulletin of Engineering Geology and the Environment 77 (2018) 1781-1791. https://doi.org/10.1007/s10064-017-1106-4.

23. L. Liu, H. Liu, A.W. Stuedlein, T.M. Evans, Y. Xiao, Strength, stiffness, and microstructure characteristics of biocemented calcareous sand, Canadian Geotechnical Journal 56(10) (2019) 1502-1513. https://doi.org/10.1139/cgj-2018-0007.

24. B. Liu, Y.-H. Xie, C.-S. Tang, X.-H. Pan, N.-J. Jiang, D.N. Singh, Y.-J. Cheng, B. Shi, Bio-mediated method for improving surface erosion resistance of clayey soils, Engineering Geology 293 (2021) 106295. https://doi.org/10.1016/j.enggeo.2021.106295.

25. S. Liu, R. Wang, J. Yu, X. Peng, Y. Cai, B. Tu, Effectiveness of the anti-erosion of an MICP coating on the surfaces of ancient clay roof tiles, Construction and Building Materials 243 (2020) 118202. https://doi.org/10.1016/j.conbuildmat.2020.118202.

26. S. Liu, J. Yu, X. Peng, Y. Cai, B. Tu, Preliminary study on repairing tabia cracks by using microbially induced carbonate precipitation, Construction and Building Materials 248 (2020) 118611. https://doi.org/10.1016/j.conbuildmat.2020.118611.

27. C. Lv, C.-S. Tang, C. Zhu, W.-Q. Li, T.-Y. Chen, L. Zhao, X.-H. Pan, Environmental dependence of microbially induced calcium carbonate crystal precipitations: Experimental evidence and insights, Journal of Geotechnical and Geoenvironmental Engineering 148(7) (2022) 04022050. https://doi.org/10.1061/(ASCE)GT.1943-5606.0002827.

28. G. Ma, Y. Xiao, W. Fan, J. Chu, H. Liu, Mechanical properties of biocement formed by microbially induced carbonate precipitation, Acta Geotechnica 17(11) (2022) 4905-4919. https://doi.org/10.1007/s11440-022-01584-8.

29. B. Montoya, J. DeJong, Stress-strain behavior of sands cemented by microbially induced calcite precipitation, Journal of Geotechnical and Geoenvironmental Engineering 141(6) (2015) 04015019. https://doi.org/10.1061/(ASCE)GT.1943-5606.0001302.

30. B.M. Montoya, J.T. DeJong, R.W. Boulanger, Dynamic response of liquefiable sand improved by microbial-induced calcite precipitation, Bio-and Chemo-Mechanical Processes in Geotechnical Engineering: Géotechnique Symposium in Print 2013, ICE Publishing, 2014, pp. 125-135. https://doi.org/10.1680/bcmpge.60531.012.

31. M.S.M. Musa, W.R.W. Sulaiman, Z.A. Majid, Z.A. Majid, A.K. Idris, K. Rajaei, Application of henna extract in minimizing surfactant adsorption on quartz sand in saline condition: A sacrificial agent approach, SN Applied Sciences 1 (2019) 1-11. https://doi.org/10.1007/s42452-019-0870-0.

32. X. Pan, J. Chu, Y. Yang, L. Cheng, A new biogrouting method for fine to coarse sand, Acta Geotechnica 15 (2020) 1-16. https://doi.org/10.1007/s11440-019-00872-0.

33. H. Salehzadeh, M. Hassanlourad, H. Shahnazari, Shear behavior of chemically grouted carbonate sands, International Journal of Geotechnical Engineering 6(4) (2012) 445-454. https://doi.org/10.3328/IJGE.2012.06.04.445-454.

34. T. Takei, K. Kato, A. Meguro, M. Chikazawa, Infrared spectra of geminal and novel triple hydroxyl groups on silica surface, Colloids and Surfaces A: Physicochemical and Engineering Aspects 150(1-3) (1999) 77-84. https://doi.org/10.1016/s0927-7757(98)00813-9.

35. D. Terzis, R. Bernier-Latmani, L. Laloui, Fabric characteristics and mechanical response of bio-improved sand to various treatment conditions, Géotechnique Letters 6(1) (2016) 50-57. https://doi.org/10.1680/jgele.15.00134.

36. D. Terzis, L. Laloui, 3-D micro-architecture and mechanical response of soil cemented via microbial-induced calcite precipitation, Scientific reports 8(1) (2018) 1416. https://doi.org/10.1038/s41598-018-19895-w.

37. L.A. van Paassen, R. Ghose, T.J. van der Linden, W.R. van der Star, M.C. van Loosdrecht, Quantifying biomediated ground improvement by ureolysis: large-scale biogrout experiment, Journal of geotechnical and geoenvironmental engineering 136(12) (2010) 1721-1728. https://doi.org/10.1061/(ASCE)GT.1943-5606.0000382.

38. K. Wang, J. Chu, S. Wu, J. He, Stress–strain behaviour of bio-desaturated sand under undrained monotonic and cyclic loading, Géotechnique 71(6) (2021) 521-533. https://doi.org/10.1680/jgeot.19.P.080.

39. Y. Wang, K. Soga, J.T. Dejong, A.J. Kabla, A microfluidic chip and its use in characterising the particle-scale behaviour of microbial-induced calcium carbonate precipitation (MICP), Géotechnique 69(12) (2019) 1086-1094. https://doi.org/10.1680/jgeot.18.P.031.

40. Y. Wang, K. Soga, J.T. DeJong, A.J. Kabla, Microscale visualization of microbial-induced calcium carbonate precipitation processes, Journal of Geotechnical and Geoenvironmental Engineering 145(9) (2019) 04019045. https://doi.org/10.1061/(ASCE)GT.1943-5606.0002079.

41. Y. Wang, K. Soga, J.T. DeJong, A.J. Kabla, Effects of bacterial density on growth rate and characteristics of microbial-induced CaCO 3 precipitates: particle-scale experimental study, Journal of Geotechnical and Geoenvironmental Engineering 147(6) (2021) 04021036. https://doi.org/10.1061/(ASCE)GT.1943-5606.0002509.

42. K. Wen, Y. Li, F. Amini, L. Li, Impact of bacteria and urease concentration on precipitation kinetics and crystal morphology of calcium carbonate, Acta Geotechnica 15 (2020) 17-27. https://doi.org/10.1007/s11440-019-00899-3.

43. P. Xiao, H. Liu, Y. Xiao, A.W. Stuedlein, T.M. Evans, Liquefaction resistance of bio-cemented calcareous sand, Soil Dynamics and Earthquake Engineering 107 (2018) 9-19. https://doi.org/10.1016/j.soildyn.2018.01.008.

44. Y. Xiao, X. He, T.M. Evans, A.W. Stuedlein, H. Liu, Unconfined compressive and splitting tensile strength of basalt fiber–reinforced biocemented sand, Journal of Geotechnical and Geoenvironmental Engineering 145(9) (2019) 04019048. https://doi.org/10.1061/(ASCE)GT.1943-5606.0002108.

45. Y. Xiao, A.W. Stuedlein, Z. Pan, H. Liu, T. Matthew Evans, X. He, H. Lin, J. Chu, L.A. Van Paassen, Toe-bearing capacity of precast concrete piles through biogrouting improvement, Journal of geotechnical and geoenvironmental engineering 146(12) (2020) 06020026. https://doi.org/10.1061/(ASCE)GT.1943-5606.0002404.

46. Y. Xiao, H. Chen, A.W. Stuedlein, T.M. Evans, J. Chu, L. Cheng, N. Jiang, H. Lin, H. Liu, H. Aboel-Naga, Restraint of particle breakage by biotreatment method, Journal of Geotechnical and Geoenvironmental Engineering 146(11) (2020) 04020123. https://doi.org/10.1061(ASCE)GT.1943-5606.0002384.

47. Y. Xiao, Y. Wang, S. Wang, T.M. Evans, A.W. Stuedlein, J. Chu, C. Zhao, H. Wu, H. Liu, Homogeneity and mechanical behaviors of sands improved by a temperature-controlled one-phase MICP method, Acta Geotechnica 16 (2021) 1417-1427. https://doi.org/10.1007/s11440-020-01122-4.

48. Y. Xiao, X. He, W. Wu, A.W. Stuedlein, T.M. Evans, J. Chu, H. Liu, L.A. van Paassen, H. Wu, Kinetic biomineralization through microfluidic chip tests, Acta Geotechnica 16(10) (2021) 3229-3237. https://doi.org/10.1007/s11440-021-01205-w.

49. Y. Xiao, X. He, A.W. Stuedlein, J. Chu, T. Matthew Evans, L.A. Van Paassen, Crystal growth of MICP through microfluidic chip tests, Journal of Geotechnical and Geoenvironmental Engineering 148(5) (2022) 06022002. https://doi.org/10.1061/(ASCE)GT.1943-5606.0002756.

50. H. Zeng, L.-Y. Yin, C.-S. Tang, C. Zhu, Q. Cheng, H. Li, C. Lv, B. Shi, Tensile behavior of bio-cemented, fiber-reinforced calcareous sand from coastal zone, Engineering Geology 294 (2021) 106390. https://doi.org/10.1016/j.enggeo.2021.106390.

51. B. Zhou, J. Wang, H. Wang, Three-dimensional sphericity, roundness and fractal dimension of sand particles, Géotechnique 68(1) (2018) 18-30. https://doi.org/10.1680/jgeot.16.P.207.

52. B. Zhou, Q. Ku, H. Wang, J. Wang, Particle classification and intra-particle pore structure of carbonate sands, Engineering Geology 279 (2020) 105889. https://doi.org/10.1016/j.enggeo.2020.105889.

53. B. Zhou, X. Zhang, J. Wang, H. Wang, J. Shen, Insight into the mechanism of microbially induced carbonate precipitation treatment of bio-improved calcareous sand particles, Acta Geotechnica (2022) 1-15. https://doi.org/10.1007/s11440-022-01625-2.

CRediT authorship contribution statement

Xing Zhang: Conceptualization, Methodology, Investigation, Visualization, Writing – original draft. **Bo Zhou**: Resources, Methodology, Writing – review & editing, Supervision. **Lingyun You**: Supervision, Writing – review & editing. **Ziyang Wu:** Data curation, Investigation. **Huabin Wang**: Resources.

Declaration of interests

☒ The authors declare that they have no known competing financial interests or personal relationships that could have appeared to influence the work reported in this paper.

☐ The authors declare the following financial interests/personal relationships which may be considered as potential competing interests: